clustering of Gly, Ser, Thr and Ala resonances in the ^{1}H-^{15}N-HSQC spectra typical of chemically denatured proteins[17,18]. All NMR data were processed using Felix95 (Biosym).

CD spectroscopy. The cytoplasmic domain of Sso1 and truncation constructs were dialyzed against 20 mM sodium phosphate buffer, pH 6.5, containing 50 mM NaCl. Protein concentrations were determined by internally standardized amino acid analysis following acid hydrolysis (performed by the W.M. Keck Foundation Biotechnology Resource Laboratory at Yale University). Far UV CD spectra were recorded on an AVIV model 62DS CD spectrometer at 15 °C in a 0.1 mm Hellma quartz cuvette between 280 nm to 200 nm. Five scans were averaged with a signal averaging time of 1 s and a step size of 1 nm. Thermal denaturation was performed in the same cuvette, with measurements taken every 2 °C between 15 and 85 °C with 2 min equilibration and 5 s signal averaging at each temperature.

Assignments. Assignments have been deposited in the BioMagResBank (BMRB) database (accession numbers 4286 and 4287 for Snc1 and Sso1, respectively).

Acknowledgments

The authors thank D. Fasshauer, L. Gonzales, R. Jahn, R.B. Sutton and S. Stallings for stimulating discussions; M. Cocco, K. Gardner and L.E. Kay for help with NMR methodology, K. Zilm for gracious access to Yale's Varian 800 MHz spectrometer, and P. Brennwald for a construct of Snc1. Support by the National Institutes of Health to A.T.B., an HHMI predoctoral fellowship to L.M.R., and a Hitchings Elion Fellowship from the Wellcome Fund to K.M.F. is gratefully acknowledged.

Correspondence should be addressed to A.T.B. *email: brunger@laplace.csb.yale.edu*

Received 11 September, 1998; accepted 19 November, 1998.

1. Ferro-Novick, S. and Jahn, R. *Nature* **370**, 191–193 (1994).
2. Weimbs, T. *et al. Proc. Nat. Acad. Sci. USA* **94**, 3046–3051 (1997).
3. Terrian, D.M. & White, M.K. *Eur. J. Cell. Biol*. **73**, 198–204 (1997).
4. Rossi, G., Salminen, A., Rice, L.M., Brunger, A.T. & Brennwald, P. *J. Biol. Chem*. **272**, 16610-16617 (1997).
5. Bennett, M.K. *Curr. Opin. Cell. Biol*. **7**, 581-586 (1995).
6. Calakos, N., Bennett, M.K., Peterson, K.E. & Scheller, R.H. *Science* **263**, 1146–1149 (1994).
7. Lin, R.C. & Scheller, R.H. *Neuron* **19**, 1087–1094 (1997).
8. Fasshauer, D., Eliason, W.K., Brunger, A.T. & Jahn, R. *Biochemistry* **37**, 10354–10362 (1998).
9. Poirier, M.A. *et al. J. Biol. Chem*. **273**, 11370–11377 (1998).
10. Sutton, R.B., Fasshauer, D., Jahn, R. & Brunger, A.T. *Nature* **395**, 347-353 (1998).
11. Fernande, I. *et al. Cell* **94**, 841–849 (1998).
12. Nicholson, K. L. *et al. Nature Struct. Biol*. **5**, 793–802 (1998).
13. Fasshauer, D., Otto, H., Eliason, W.K., Jahn, R. & Brunger, A.T. *J. Biol. Chem*. **272**, 28036–28041 (1997).
14. Fasshauer, D., Bruns, D., Shen, B., Jahn, R. & Brunger, A.T. *J. Biol. Chem*. **272**, 4582–4590 (1997).
15. Rice, L.M., Brennwald, P. & Brunger, A.T. *FEBS Lett*. **415**, 49–55 (1997).
16. Schulman, B.A., Kim, P.S., Dobson, C.M. & Redfield, C. *Nature Struct. Biol*. **4**, 630–634 (1997).
17. Schwalbe, H. *et al. Biochemistry* **36**, 8977–91 (1997).
18. Wishart, D.S., Bigam, C.G., Holm, A., Hodges, R.S. & Sykes, B.D. *J. Biomol. NMR* **5**, 67–81 (1995).
19. Hanson, P.I., Roth, R., Morisaki, H., Jahn, R. & Heuser, J.E. *Cell* **90**, 523–535 (1997).
20. Hanson, P.I., Otto, H., Barton, N. & Jahn, R. *J. Biol. Chem*. **270**, 16955–16961 (1995).
21. Aalto, M.K., Ronne, H. & Keranen, S. *EMBO J*. **12,** 4095–4104 (1993).
22. Hata, Y., Slaughter, C.A. & Südhof, T.C. *Nature* **366**, 347–351 (1993).
23. Garcia, E.P., McPherson, P.S., Chilcote, T.J., Takei, K. & De Camilli, P. *J. Cell. Biol*. **129**, 105–120 (1995).
24. Pevsner, J., Hsu, S.C. & Scheller, R.H. *Proc. Natl. Acad. Sci. USA* **91**, 1445–9 (1994).
25. Kay, L.E., Keifer, P. & Saarinen, T. *J. Am. Chem. Soc*. **114**, 10663–10665 (1992).
26. Live, D.H., Davis, D.G., Agosta, W.C. & Cowburn, D. *J. Am. Chem. Soc*. **106**, 1939–1943 (1986).
27. Marion, D. *et al. Biochemistry* **28**, 6150–6156 (1989).
28. Driscoll, P.C., Clore, G.M., Marion, D., Wingfield, P.T. & Gronenborn, A.M. *Biochemistry* **29**, 3542–3556 (1990).
29. Bartels, C., Xia, T.H., Billeter, M., Guntert, P. & Wüthrich, K. *J. Biomol. NMR* **6**, 1–10 (1995).
30. Zhang, O., Kay, L.E., Olivier, J.P. & Forman-Kay, J.D. *J. Biomol. NMR* **4**, 845–858 (1994).

Structural basis for HLA-DQ binding by the streptococcal superantigen SSA

Eric Sundberg and Theodore S. Jardetzky

Department of Biochemistry, Molecular Biology and Cell Biology, Northwestern University, Evanston Illinois 60208, USA.

Streptococcal superantigen (SSA) is a 28,000 M_r toxin originally isolated from a pathogenic strain of *Streptococcus pyogenes* that has 60% sequence identity with staphylococcal enterotoxin B (SEB). SSA and SEB, however, do not compete for binding on the surfaces of cells expressing MHC class II molecules. This behavior had been ascribed to SSA and SEB binding to distinct sites on, or different subsets of, HLA-DR molecules. Here we demonstrate that SSA binds predominantly to HLA-DQ, rather than to HLA-DR molecules, and present the crystal structure of SSA at 1.85 Å resolution. These data provide a structural basis for interpreting the interaction of SSA with HLA-DQ molecules as well as a foundation for understanding bacterial superantigen affinities for distinct MHC isotypes.

Bacterial superantigens (bSAgs) bind as folded proteins to both major histocompatibility complex (MHC) class II molecules on the surfaces of antigen-presenting cells and T cell receptor Vβ domains on T cells[1,2]. The resulting activation of T cells correlates with a number of human diseases, including food poisoning and toxic shock syndrome, and may play an important role in autoimmune diseases[2–4]. Although bSAgs share highly homologous sequences, as well as similar three-dimensional folds, binding to MHC class II molecules depends on the biochemical and structural states of class II molecules expressed on the cell surface. Understanding the molecular basis for bSAg–MHC affinities and specificities may provide fundamental insights into MHC function as well as the role of superantigens in disease.

The cocrystal structures of SEB[5] and toxic shock syndrome toxin-1[6] (TSST-1), complexed with the class II molecule HLA-DR1, show that these two superantigens have overlapping MHC binding sites, although functional studies show that they do not compete for MHC class II binding on all DR1 molecules. Although bSAgs bind outside of the conventional MHC–peptide binding site, the affinity of the bSAg–MHC interaction is affected by peptides bound to the MHC molecule[7]. This was first demonstrated for the bSAgs staphylococcal enterotoxin A (SEA) and TSST-1, which may both interact directly with MHC-bound peptides[8]. More recently, binding studies using cell lines expressing various components of the antigen-processing machinery (invariant chain [Ii] and HLA-DM) have shown that the interaction of SEB, SEA and TSST-1 to HLA-DR is dependent on the particular processing machinery of the MHC-expressing cell line and, subsequently, what is displayed in the class II binding groove on the cell surface[9].

SEB and the streptococcal superantigen SSA are highly homologous (60% identity); however, these two toxins do not compete with each other for binding on a variety of cell lines expressing HLA-DR[10]. Like SEB, SSA interacts with αLys 39 of MHC class II molecules and has a comparable hydrophobic ridge, although subtle amino acid differences could promote an altered SSA–MHC binding interaction. In light of the recently determined role that the cellular peptide-processing machinery plays in bSAg binding[9], the lack of competition between SSA and SEB binding could also be due to the abilities of these bSAgs to bind distinct (poly)peptide-loaded subsets of HLA-DR on the surface of cells. It is also consistent, however, with the preferential binding of SSA and SEB to different class II isotypes on the cell surface. Several group A *Streptococcus*-derived superantigens have been shown to require HLA-DQ for superantigenic activity, such as SpeA and SpeC[11], SpeF[12] and a protein from the peptic extract of type 12 group A streptococci, PEAST12[13].

Here we show that SSA binds specifically to HLA-DQ1 molecules expressed on the cell surface of LG2 cells, and not to HLA-DR molecules, explaining the lack of competitive binding between SSA and SEB. We have resolved the crystal structure of SSA to high resolution, allowing us to analyze this binding preference using the three-dimensional structure of SSA and related bSAgs. This analysis provides the first structural insights into the evolution of bSAg specificity for MHC isotypes and provides a model for further understanding the interactions of this family of proteins with MHC class II molecules.

SSA binds HLA-DQ on the cell surface

SSA binding to a panel of cell types expressing different subsets of class II molecules was tested. Specific binding of ^{125}I-labeled SSA was detected on the B cell lines LG2, Raji, 45.1, and SA (Fig. 1*a*). This binding could be effectively competed by the addition of excess unlabeled SSA. No significant binding to any transfected cell lines expressing HLA-DR1 or DR3 was detected (Fig. 1*a*). This panel of cell lines expressing HLA-DR produces cell surface MHC class II molecules loaded with distinct (poly)peptides, including large cellular polypeptides (HeLa-DR1, DAP-DR1); CLIP (T2-DR) and full-length Ii (HeLa-DR1 / Ii); as well as fully processed cellular peptides (T2-DR3 / DM)[14]. Control experiments with SEA, SEB and TSST-1 showed that the transfected cell lines used in this study were able to bind these bSAgs as demonstrated previously[9].

In contrast to SSA, SEB bound transfected cell lines (HeLa-DR1) but not B cells (LG2), and therefore no competition between SSA and SEB was seen on either of these cell types (Fig. 1*b*). In order to determine if SSA and SEB share an overlapping binding site on HLA-DR1 expressed in different cell lines, the monoclonal antibody (mAb) L243 was used in competition assays. L243 blocks ^{125}I-labeled SEB binding to HeLa-DR1 cells but not the binding of SSA to LG2 cells. In order to test whether SSA might bind to another region of HLA-DR1, a polyclonal antibody (pAb) (CHAMP) was used to compete the binding of SSA and SEB to LG2 and HeLa-DR1 cells, respectively. SSA binding was not significantly inhibited by high levels of CHAMP, while SEB binding was effectively blocked by CHAMP addition.

These experiments suggest that the majority of SSA binding to LG2 cells must be directed to molecules other than HLA-DR on the cell surface. SSA has been shown to proliferate T cells using HLA-DQ-transfected cell lines[15]. Therefore, an anti-HLA-DQ1, -DQ2 and -DQ3 monoclonal antibody (Tü169) was tested as an inhibitor of ^{125}I-labeled SSA binding. Tü169 effectively competed with SSA binding to LG2 cells but had no significant effect on SEB binding to HeLa-DR1 cells (Fig. 1*b*). Because LG2 cells are homozygous for HLA-DQ1, the L243 and Tü169 competition experiments indicate that SSA binds predominantly to HLA-DQ1 on the LG2 cell surface. SSA binds to other HLA-DQ alleles, as shown by the specific binding of ^{125}I-labeled SSA to Raji cells (Fig. 1*a*), which express a different HLA-DQ α-chain from that found in LG2 cells.

SSA shares the canonical bacterial superantigen fold

The SSA crystal structure was determined by molecular replacement methods using SEC3[16] as a model and was refined as described in the Methods. Crystallographic and refinement statistics are shown in Table 1 and a region of the refined $|2F_o - F_c|$ elec-

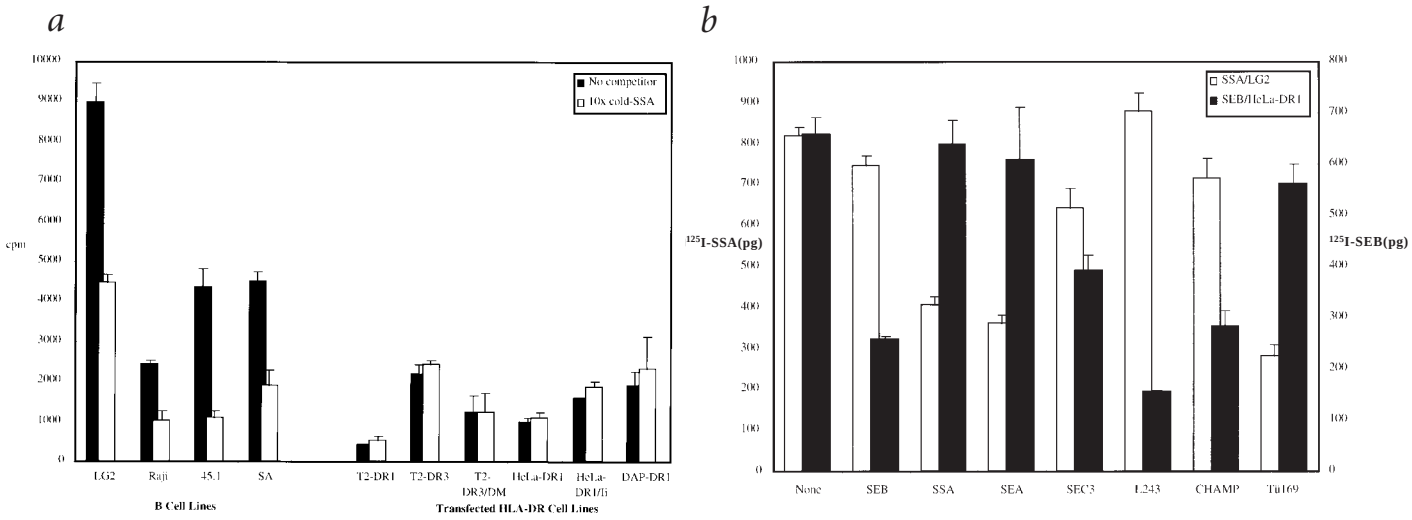

Fig. 1 SSA and SEB binding to MHC class II-expressing cell lines. ***a***, 100 ng of ^{125}I-labeled SSA was incubated with 10^6 cells with or without a 10-fold excess of cold SSA in binding assays described in the Methods. Unlabeled SSA inhibits the binding of ^{125}I-SSA to the B cell lines (LG2, Raji, 45.1 and SA), whereas there is no specific SSA binding to any other class II-expressing cell line. ***b***, 100 ng of ^{125}I-SSA were incubated with 10^6 LG2 cells, and 100 ng of ^{125}I-SEB were incubated with 10^6 HeLa-DR1 cells, with or without a 10-fold excess of various competitors. SSA and SEB do not compete with each other in binding to class II-expressing cell lines and are differentially affected by the bSAgs SEA and SEC3 as well as the antibodies L243 (anti-DR1 mAb), CHAMP (anti-DR1 pAb) and Tü169 (anti-DQ1,2,3 mAb).

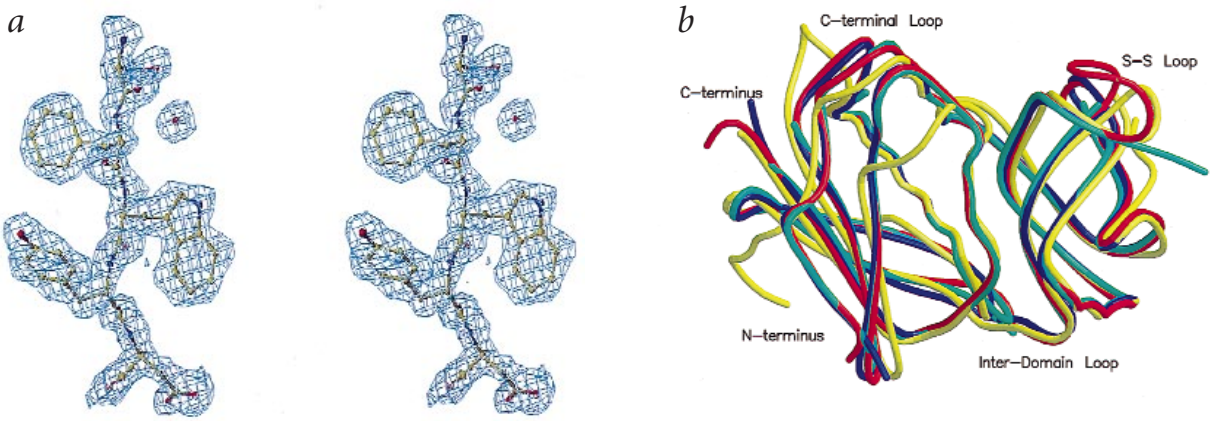

Fig. 2 Crystallographic analysis of the refined SSA structure. ***a***, $|2F_o - F_c|$ electron density map of a region of the final SSA model, including residues Ser 192, Phe 193, Trp 194, Tyr 195 and Asp 196, as well as a water molecule. The map was calculated using the program X-PLOR[27] with combined phases from the program SIGMAA[26] and contoured at 1.2σ. The map and model were displayed in O[28]. ***b***, Comparison of bacterial superantigen backbone structures. Structural alignments using only Cα atoms were performed using O[28], and were displayed using the program SETOR[29]. SSA is shown in red, SEB in blue, SEA in green and SEC3 in purple. Domain 1, the MHC binding domain, is on the right, and domain 2 is on the left. Labels refer to loops that differ significantly in structure between the bSAgs, as discussed in the text.

tron density map is shown in Fig. 2*a*. The structure of SSA conforms generally to that of other bSAgs and comprises two domains of αβ structure. SSA is highly homologous to SEB, SEC3 and SEA, and indeed, its structural similarity is also very high with these bSAgs (Fig. 2*b*). The only regions that differ significantly in structure between these bSAgs are restricted to (i) the disulfide loop region, (ii) the loop following the α-helix in the C-terminal region and (iii) the interdomain loop.

Superantigen-MHC class II interfaces

Three distinct classes of bSAg–MHC complexes have been characterized, including the SEB–DR1[5] and TSST-1–DR1[6] cocrystal structures and a zinc-mediated SEA–MHC class II complex[17,18]. Independent lines of evidence strongly suggest that SSA forms a complex with HLA-DQ molecules that is most similar to the SEB–DR1 complex. The crystal structure and sequence of SSA are more closely related to SEB and SEA as compared to TSST-1 in the MHC class II N-terminal binding regions of the bSAgs (Fig. 3*a*). Purified SSA does not contain zinc, as determined by atomic adsorption spectroscopy, and the zinc-binding site of SEA (His 187, His 225 and Asp 227) is absent in SSA (corresponding residues Ile 186, Ala 226 and Glu 228). The SSA crystal structure and mutational studies together also suggest that SSA has a functional SEB-like binding surface for MHC class II molecules. The SEB binding site for MHC molecules has two major structural features: a polar pocket that binds the HLA-DR1 αLys 39 and a hydrophobic ridge that binds the MHC class II α-chain between two loops of the β-sheet. There is a reasonable degree of sequence conservation between this class II binding site of SEB and its analog on SSA (Fig. 3*a*).

Although SSA binding to HLA-DR is weak compared to that for HLA-DQ, HLA-DR1 can still present SSA in T cell activation studies. Mutation of αLys 39 of HLA-DR1 diminishes T cell activation by SSA compared to a wild-type DR1 background[10]. In the SEB–DR1 crystal structure[5], αLys 39 forms a salt bridge with three SEB side chains. These conserved residues in SSA (Glu 67, Tyr 89 and Tyr 110) are found in nearly identical conformations, which could allow a similar interaction with the class II molecule (Fig. 3*a,b*). The neighboring hydrophobic ridge residues of SSA and SEB are also similar, although there is a significant volume reduction and fewer hydrophobic residues in the SSA ridge (Fig. 3*a,c*). The ridge of SSA is more polar because of the substitutions of a glutamine for a tyrosine at residue 46 and a histidine for a phenylalanine at residue 47. Simultaneous mutation of the residues 44–47 in SSA to the corresponding residues found in SEB reduces the inhibition of labeled SSA binding to LG2 cells[10]. Therefore, both the polar pocket and hydrophobic ridge regions of SSA are directly implicated in MHC class II interactions.

The HLA-DQ structure, though not determined to atomic detail, is likely to be similar to that of HLA-DR. The αLys 39 residue of HLA-DR1 that forms a salt bridge with SEB is conserved in all HLA-DQ molecules, consistent with the formation of an SSA–DQ1 complex similar to SEB–DR1[5]. However, there are several sequence differences between HLA-DR and DQ in the bSAg binding region, including residues surrounding αLys 39 as well as those within the MHC class II cleft that accommodates the hydrophobic ridge of SEB (residues 17, 18, 36–38, 55, 61 and 63; Fig. 3*a*). These differences constitute nearly half of the entire bSAG binding region and could play a role in the binding preferences of SSA and SEB for their respective MHC class II binding partners.

SSA residues that confer affinity, specificity for HLA-DQ

The residues of SSA within the proposed MHC class II binding site are shown in Fig. 4*a*. Residues that are conserved in SSA and SEB, or that have been shown by mutational analysis[10] to have little effect on SSA binding affinity to HLA-DQ1, are shown in gray (the polar pocket and the majority of the hydrophobic ridge). Two residues of the SSA hydrophobic ridge (Gln 46 and His 47), which differ in SSA and SEB and are partially, but not completely, responsible for switching the MHC isotype binding preference of SSA, are shown in red. Mutation of residues 44–47 in SSA (Leu-Leu-Gln-His) to the corresponding SEB residues (Phe-Leu-Tyr-Phe) reduces SSA binding to HLA-DQ, whereas the point mutation, L44F, has no effect[10].

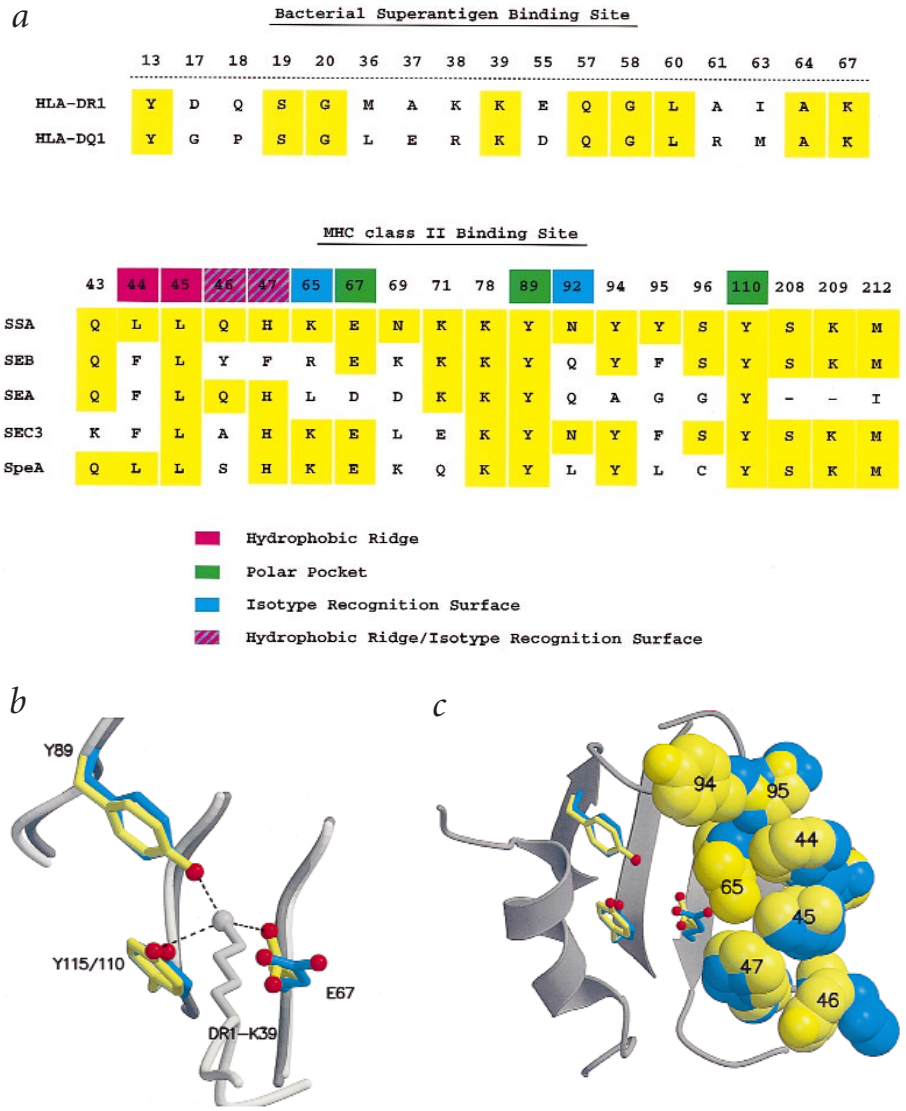

Fig. 3 Structural comparisons of the MHC class II binding motifs in SEB and SSA. ***a***, Sequence alignment of the bSAg binding domain of HLA-DR1 and DQ1 and the MHC class II binding regions of the bSAgs SSA, SEB, SEA, SEC3 and SpeA (numbering corresponds to SSA). Conserved residues are shown in yellow. ***b***, Overlay of the polar pocket regions of SEB (side chains in yellow, Cα backbone in light gray) and SSA (side chains in cyan, Cα backbone in dark gray) shows nearly identical geometry of the salt bridge formed by DR1-αLys 39 (side chain in gray) and the conserved polar residues in the bSAg binding domain (Glu 67, Tyr 89 and Tyr 115 [Tyr 110 in SSA]). ***c***, Overlay of the class II binding domain of SEB and SSA. Color coding is the same as in (*a*). The polar pocket residues are represented in ball-and-stick form and are placed in the figure for reference. Side chains of residues in the hydrophobic ridge are represented in CPK space-filling form in order to highlight the volumetric differences between SEB and SSA in this region of the binding domain. The side chain of SSA Tyr 94 has been omitted for visual clarity as it points away from the class II molecule, although a change in rotamer conformation upon MHC binding could place it in an identical conformation to that of SEB Tyr 94. Parts (*b*) and (*c*) generated using MOLSCRIPT[30].

The majority of residues in this region, including the three residues that form the polar pocket and those forming the backside, noninteracting portion of the hydrophobic ridge, are not critical for HLA-DQ binding. Since residues 46 and 47 are only partially responsible for the SSA binding preference for class II molecules, other residues must be involved. Residues that differ between SSA and SEB in this region that may contribute to HLA-DQ binding are shown in yellow in Fig. 4*a* (Lys 65, Asn 69, Asn 92 and Tyr 95). Of these four residues, only SSA Lys 65 is located at the center of the MHC class II binding site and is thus most likely to contribute significantly to the binding energy of the interaction[19]. Residue 95 has an aromatic side chain that points away from the MHC class II binding site in both the SSA and SEB crystal structures, and is not likely to play a direct role in HLA-DQ binding. SSA residues Asn 69 and Asn 92 are substitutions of Lys 69 and Gln 92 of SEB, but these residues lie at the periphery of the MHC class II binding site.

The substitution of Lys 65 in SSA for Arg 65 in SEB changes the binding site in two ways. The smaller lysine side chain, relative to that of arginine, could affect the packing at the bSAg–MHC class II interface (Fig. 3*c*). The hydrogen-bonding characteristics of these two residues also differ in SEB and SSA. Arg 65 in SEB makes three hydrogen bonds through its guanidinium group to Tyr 94, Glu 67 and Asp 48 (Fig. 4*b*), while SSA Lys 65 can form only a single weak hydrogen bond to Glu 67 (Fig. 4*c*).

Implications for other bSAg–MHC class II interactions

Five residues are implicated in conferring HLA-DQ1 binding specificity to SSA as compared to SEB (Gln 46, His 47, Lys 65, Asn 69 and Asn 92). Since SSA, SEC3, SEA and SpeA have all been shown to bind HLA-DQ, comparison of their sequences (Fig. 3*a*) may reveal additional information on the specificity of the bSAg–MHC class II interactions. Residues Gln 46, His 47, Lys 65, Asn 69 and Asn 92 each are found in two, four, three, one and two of these four bSAgs, respectively. His 47 and Lys 65 are the most conserved differences from SEB in the bSAgs that bind HLA-DQ molecules, followed by Gln 46 and Asn 92. Residue 69 is different in all four of these bSAgs. Because residues 46, 47, 65 and 92 are different between SSA and SEB, share degrees of similarity between SSA and those bSAgs that compete with it for HLA-DQ binding, and are highly polymorphic among all known bSAgs, they serve as

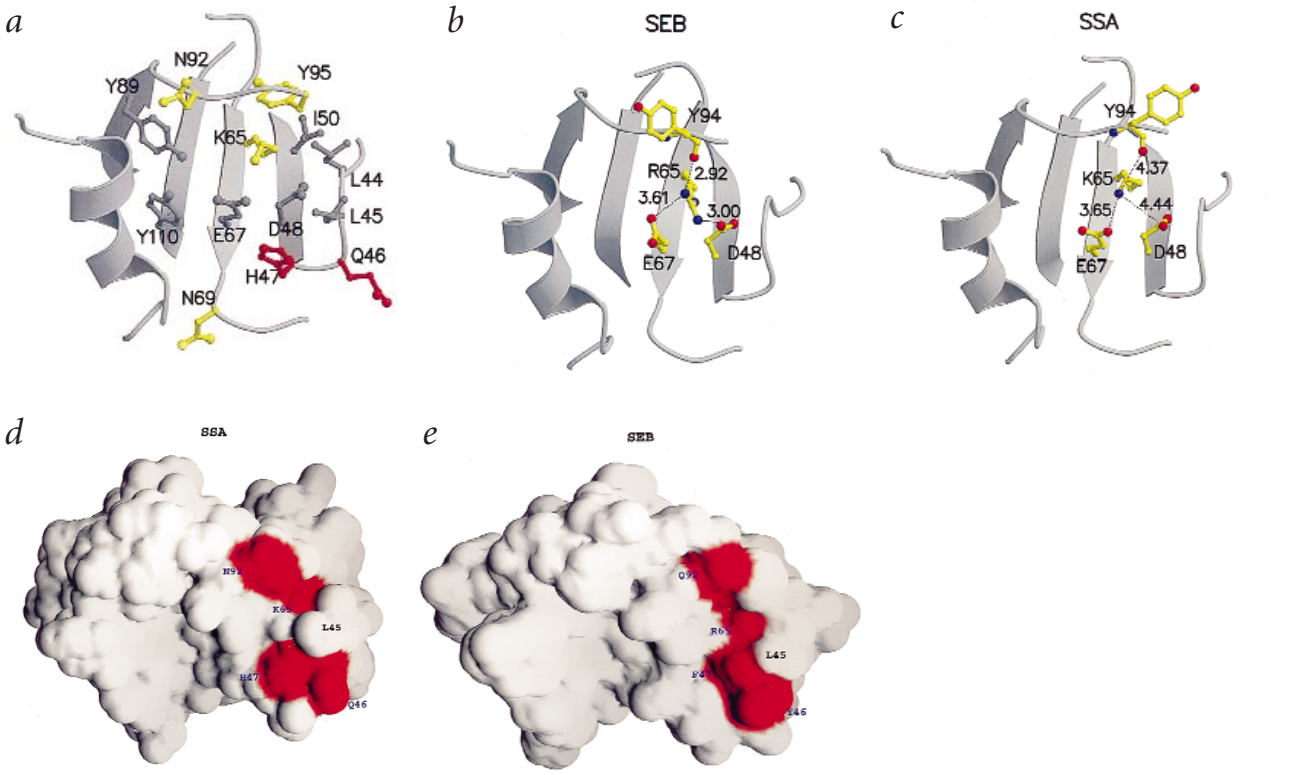

Fig. 4 SSA residues responsible for HLA-DQ affinity and specificity. ***a***, Residues in the MHC class II binding region of SSA that are the same between SSA and SEB or have no effect on SSA or SEB specificity[10] (Leu 44, Leu 45, Asp 48, Leu 49, Ile 50, Phe 51, Pro 52, Glu 67, Tyr 89 and Tyr 110) are shown in gray; residues implicated in affecting the affinity of SSA for MHC class II molecules from mutational studies (Gln 46 and His 47) are shown in red; and residues in this region that differ between SSA and SEB (Lys 65, Asn 69, Asn 92 and Tyr 95) are shown in yellow; generated with MOLSCRIPT[30]. The following is a summary of a series of investigations of the MHC binding properties of SSA by mutational analysis[10].The SSA triple mutant (E67A, Y89A, Y110A) and SSA single mutant (44SEB, L44F) compete labeled-SSA binding similarly to wild-type SSA[10], showing that these residues are not critical for SSA binding. The SSA/SEB hybrid mutants (44–47SEB) or (44–52SEB) compete labeled-SSA binding to LG2 cells at a level intermediate between that of wild-type SSA and SEB. This suggests that the C-terminal end of the hydrophobic ridge of SSA and SEB (residues 46 and 47, but not 48–52) are partially responsible for class II binding preference. ***b***, Arg 65 of SEB forms intramolecular hydrogen bonds with Asp 48, Glu 67 and Tyr 94. Interatomic distances are in Å. ***c***, Arg 65 of SSA makes only one intramolecular hydrogen bond, to Glu 67. Residues Asp 48 and Tyr 94 are located at too great a distance from Lys 65 to form appropriate hydrogen-bonding interactions, indicated by the interatomic distances in Å. ***d***, The MHC class II binding domain of SSA. GRASP[31] surface representation highlighting in red SSA residues (Gln 46, His 47, Lys 65 and Asn 92, where Asn 92 is modeled as an alanine because its disorder in the crystal did not allow model building of the asparagine side chain) that are implicated in determining the specificity of SSA for HLA-DQ molecules. **e,** The MHC class II binding domain of SEB. GRASP[31] surface representation of SEB as in (*d*). The residues highlighted in red include Tyr 46, Phe 47, Arg 65 and Gln 92.

excellent candidates for the key determinants in MHC class II isotype specificity.

The four SSA residues Gln 46, His 47, Lys 65 and Asn 92 form a nearly contiguous surface spanning the C-terminal portion of the hydrophobic ridge, the space between the ridge and polar pocket as well as the segment of loop region along the upper face of the pocket (Fig. 4*d*). Residues Lys 65 and His 47 are most central to the MHC binding site and most conserved in bSAgs that bind HLA-DQ. This molecular region may act as an isotype recognition surface predominantly responsible for MHC isotype binding preference. The corresponding four residues in SEB are shown in Fig. 4*e*. The substitution of Arg 65 in SEB by Lys 65 in SSA results in a topological change in the class II binding region. In relation to Leu 45 (conserved in both SEB and SSA), Lys 65 creates a more concave surface in SSA than does Arg 65 in SEB, altering significantly the structure of the MHC binding surface.

This isotype recognition surface interacts with several polymorphic regions of the MHC molecule when the SSA–DQ1 interaction is modeled on the DR1–SEB structure[5]. SEB Tyr 46 (Gln 46 in SSA) interacts with residue α18 of the class II molecule, which is mutated from a glutamine in HLA-DR1 to a proline in HLA-DQ1 (Fig. 3*a*). A possible effect of this mutation would be a conformational change of the DQ1 β-strand, altering the hydrophobic cleft of the MHC molecule and its potential interaction with SSA residues 47 and 65. Residue 65 is also located near the polymorphic MHC residue α36. The change of Arg 65 in SEB to Lys 65 in SSA would create a large cavity at the bSAg–MHC interface, which could be filled by water molecules or compensated by additional structural changes at the binding interface.

The crystal structures of murine MHC class II I-A/peptide[20,21] reveal two structural features not found in HLA-DR or I-E molecules that may be present in HLA-DQ molecules. The first is a β-bulge in the I-A α-chain that is caused by an insertion of a glycine in the β_1 strand, conserved in HLA-DQ sequences. Although the glycine is located far from the bSAg binding site, it may still propagate a structural change to the putative SSA binding region. The second feature observed in the I-A^d/peptide structures is a movement of the α_1 domain α-helix by ~1.2 Å toward the center of the peptide binding groove[21]. This movement of the α-helix may be caused, in part, by αPro 56, which is also conserved in

Table 1 Data collection and refinement statistics[1]

Resolution limit (Å)	1.85	
Mosaicity (°)	0.8	
R_{merge} (%)[2]	8.3 (31.9)	
Unique reflections	35,601	
Total observations	150,778	
Completeness (%)	82.9 (79.4)	
Refinement		
R_{free}[3]	26.3	
R_{cryst}	23.7	
	Residue	Average B
Protein	448	16.7
Water	380	29.9
R.m.s. deviations		
Bonds (Å)	0.008	
Angles (°)	1.676	

[1]Values in parentheses correspond to the highest resolution shell (1.88–1.85 Å).
[2]$R_{merge} = \Sigma | I - \langle I \rangle | / \Sigma \langle I \rangle$, where I is the observed intensity and <I> is the average intensity of multiple observations of symmetry-related reflections.
[3]A total of 5% of the overall reflections were set aside for R_{free} calculations in resolution shells such that all noncrystallographic symmetry-related reflection pairs would be used only in either the working set or the free set, in order to reduce bias in the calculation of R_{free}.

HLA-DQ sequences. Movement of this helical region would directly alter the structure of the bSAg binding pocket on the α_1 domain.

Bacterial superantigens clearly have evolved a wide range of interactions with MHC class II molecules that can be sensitive to MHC polymorphisms and bound (poly)peptides. Here we have elucidated the structural basis by which particular MHC isotypes present on the cell surface also play a distinct role in these interactions. We have shown that SSA binds well to HLA-DQ1 molecules, but not to HLA-DR molecules. The binding region on MHC molecules for SSA and SEB is not only polymorphic between HLA-DR and -DQ isotypes but also between individual HLA-DQ alleles. Although SSA binds preferentially to HLA-DQ1 on the surface of LG2 cells (which expresses the α-chain allele DQA1*0101), and to HLA-DQA4.1 molecules on the surface of Raji cells (α-chain allele DQA1*0501), it is unlikely that SSA binds equally to all HLA-DQ alleles; such a scenario probably holds true for all bSAgs that bind HLA-DQ. This raises the possibility that the preferential interaction of bSAgs with different MHC alleles may contribute to the pathogenicity of these proteins. In particular, bSAg binding to specific HLA-DQ alleles may be important in understanding HLA-DQ associations with distinct autoimmune diseases. The results presented here provide a structural foundation for further exploration of the specificity of bSAg–MHC interactions.

Methods

Protein expression and purification. An SSA–glutathione *S*-transferase (GST) fusion protein-expressing *Escherichia coli* strain was a gift. Recombinant SSA was overexpressed and purified as described[10]. Briefly, XL-1 Blue Super-competent *E. coli* transformed with a pGEX-2T vector (Stratagene), expressing SSA as a fusion protein with GST, were used to inoculate 200 ml 2×YT/10% glucose/100 mg ml^{-1} ampicillin and incubated overnight at 37 °C, 250 r.p.m. Two liters of this medium were inoculated with the overnight cultures and grown to a cell density of OD_{600} = 1.0 under the same growth conditions. Cells were induced with IPTG (Fisher) at a final concentration of 1 mg ml^{-1} for 4 h, after which they were pelleted and resuspended in 100 ml cold TSE buffer (50 mM Tris, 100 mM sucrose, and 10 mM EDTA, pH 8.0). Lysozyme (Sigma) at a final concentration of 0.5 mg ml^{-1} and protease inhibitors [0.03 mg ml^{-1} aprotinin, 0.04 mg ml^{-1} bestatin, 0.01 mg ml^{-1} leupeptin (Sigma) and 1 mM PMSF (Research Organics)] were added and the cells incubated on ice for 30 min. The cells were lysed by sonication and 10% Triton X-100 (Fisher) was added for 10 min. Lysates were cleared of cellular debris by centrifugation and of any remaining lipids by ultracentrifugation. The SSA–GST fusion protein was purified over a glutathione–sepharose column (Pharmacia), and cleaved by incubation with trypsin-agarose beads (Sigma) (0.7 units mg^{-1} SSA–GST) at 25 °C for 3 h. The reaction was terminated by adding 25 ng trypsin inhibitor (Sigma) per unit trypsin and the trypsin–agarose removed by filtration through a 0.22 μm filter. The cleaved product was passed over the glutathione–sepharose column multiple times to ensure the complete separation of SSA from GST.

Binding assays. For binding assays, 20 μg of SSA or SEB were incubated with 0.5 μg iodogen (Pierce) and 250 μCi ^{125}I (ICN) for 10 min at room temperature. The radiolabeled toxins were separated from free iodide using a De-Salt column (Pierce) blocked with 0.1% BSA. The binding assays were performed as described in ref. 9. Briefly, 10^6 cells were incubated in DMEM/2% FBS/0.02% NaN_3 with 100 ng ^{125}I-labeled superantigen in the presence or absence of a 10-fold excess of cold superantigen or antibody, at 37 °C for 4 h. HeLa and DAP cells were cultured in DMEM/5% FBS/0.1% Gentamicin; B cell lines and T2 cells were cultured in RPMI/10% CS/0.1% Gentamicin/0.02% BME. SEB (Sigma), SEA (Sigma), SEC3 (Toxin Technologies) and Tü169 (Pharmingen) were purchased. L243 was produced by the Northwestern University Monoclonal Antibody Facility and CHAMP was a gift. The cell–superantigen mixture was overlayed onto silicon–mineral oil (84:16) and centrifuged at 8,000*g* for 5 min. This forces the cells to migrate through the oil mixture to the bottom of the tube while unbound superantigen remains in the supernatant. Tubes were frozen briefly at –80 °C and the ends clipped off in order to determine radioactivity levels.

Crystallization and data collection. SSA (10 mg ml^{-1}) was crystallized by hanging-drop vapor diffusion in 100 mM sodium cacodylate (Sigma), pH 6.5, 50–200 mM magnesium acetate (Fluka), and 15–23% PEG 8000 (Fluka) at 4 °C. The crystals belong to the space group $C222_1$, with cell dimensions of a = 81.90 Å, b = 84.55 Å, and c = 144.01 Å. There are two molecules in the asymmetric unit, resulting in an approximate solvent content of 51%. Crystals were frozen by incubating in mother liquor plus 30% glycerol (Eastman Kodak) for 1 min, and then dunking immediately into liquid propane. Two native data sets were collected, one each at 4 °C using a rotating Cu anode X-ray source (Rigaku) and a multiwire area detector (Siemens), and at –160 °C at Brookhaven National Laboratory, National Synchrotron Light Source, beamline X-25A using a 300 mm image plate detector (Mar Research).

Structure refinement. The data were processed using XDS[22] and the HKL programs DENZO and SCALEPACK[23]. Molecular replacement methods, using the program AMoRe[24], were applied to obtain initial phases with SEC3[16] as a search model. The initial rotation and translation function searches were carried out over the resolution range of 20–3.4 Å. The top four solutions from the rotation function had correlation coefficients of 0.099–0.107 (6.5–7.1σ above the mean). These solutions were used in the translation function search and gave two symmetry-related solutions each, with correlation coefficients of 0.533 and R-factors of 0.433. The density modification program DM[25] was used to average density between the two molecules in the asymmetric unit, and SIGMAA[26] was used for phase recombination. Iterative rounds of positional, simulated annealing, individual temperature factor refinement and bulk solvent correction using X-PLOR[27], and manual model building using O[28] were carried out. Simulated annealing omit maps, in which stretches of 20 amino acids were omitted, were produced using X-PLOR[27] periodically throughout the refinement process in order to evaluate the validity of the model and corresponding electron density. The two molecules in the asymmetric unit were initially constrained tightly

by noncrystallographic symmetry, but were refined individually in the final stages of refinement. In the final model, these two molecules have an r.m.s. deviation of 0.157 Å. A total of 380 noncrystallographic symmetry-related water molecules were added to the final model. Due to poor density, the majority of the disulfide loop, from residues 96–105 could not be built, and the residues Lys 54, Lys 57 and Asn 92 were modeled as alanine. In a Ramachandran plot, 90.3% of the residues were found in their preferred regions, with no residues lying in disallowed regions.

Coordinates. The atomic coordinates of SSA have been deposited in the Protein Data Bank (accession code 1bxt).

Acknowledgments

We thank K.R. Stevens and R. Rich for the kind contribution of the SSA-expressing *E. coli* strain, L. Gu for the L243 antibody, D. Wiley for the CHAMP antibody, L. Bermann for assistance at the BNL-NSLS X-25A beamline, as well as P. Lavoie and R-P. Sékaly for provision of cell lines and for hosting E.S. in the Sékaly laboratory (Montreal, Quebec, Canada) in order to learn the experimental techniques of the cell binding assay. We also thank S. Garman and P. Lavoie for careful reading of, and editorial comments on, the manuscript. E.S. is supported by a grant from the NIH. This work has been funded by a grant from the NIH and an award from the Human Frontier Science Program.

Correspondence should be addressed to T.S.J. *email: jardetz@tochtli.biochem.nwu.edu*

Received 7 July, 1998; accepted 3 November, 1998.

1. Scherer, M.T. *et al. Ann. Rev. Cell Biol.* **9**, 101–128 (1993).
2. Kotzin, B.L., Leung, D.Y., Kappler, J. & Marrack, P. *Adv. Immunol.* **54**, 99–165 (1993).
3. Conrad, B. *et al. Cell* **90**, 303–313 (1997).
4. Renno, T. & Acha-Orbea, H. *Immunol. Rev.* **154**, 175–191 (1996).
5. Jardetzky, T.S. *et al. Nature* **368**, 711–718 (1994).
6. Kim, J., Urban, R.G., Strominger, J.L. & Wiley, D.C. *Science* **266**, 1870–1874 (1994).
7. Kozono, H., Parker, D., White, J., Marrack, P. & Kappler, J. *Immunity* **3**, 187–196 (1995).
8. Thibodeau, J. *et al. Science* **266**, 1874–1878 (1994).
9. Lavoie, P.M. *et al. Proc. Natl. Acad. Sci. USA* **94**, 6892–6897 (1997).
10. Stevens, K.R., Van, M., Lamphear, J.G. &nd Rich, R.R. *J. Immunol.* **157**, 4970–4978 (1996).
11. Toyosaki, T. *et al. Eur. J. Immunol.* **26**, 2693–2701 (1996).
12. Norrby-Teglund, A. *et al. Infect. Immun.* **62**, 5227–5233 (1994).
13. Esaki, Y. *et al. Infect. Immun.* **62**, 1228–1235 (1994).
14. Busch, R., Cloutier, I., Sékaly, R.-P. & Hämmerling, G.J. *EMBO J.* **15**, 418–428 (1996).
15. Mollick, J.A. *et al. J. Clin. Invest.* **92**, 710–719 (1993).
16. Deringer, J.R., Ely, R.J., Stauffacher, C.V. & Bohach, G.A. *Mol. Microbiol.* **22**, 523–534 (1996).
17. Abrahmsén, L. *et al. EMBO J.* **14**, 2978–2986 (1995).
18. Hudson, K.R. *et al. J. Exp. Med.* **182**, 711–720 (1995).
19. Clackson, T. & Wells, J.A. *Science* **267**, 383–386 (1995).
20. Fremont, D.H. *et al. Immunity* **8**, 305–317 (1998).
21. Scott, C.A., Peterson, P.A., Teyton, L. & Wilson, I.A. *Immunity* **8**, 319–329 (1998).
22. Kabsch, W. *J. Appl. Crystallogr.* **21**, 916 (1988).
23. Otwinowski, Z. *Data collection and processing* (Warrington, UK; 1993).
24. Navaza, J. *Acta Crystallogr. A***50**, 157–163 (1994).
25. Collaborative Computational Project No. 4. *Acta Crystallogr. D***50**, 760–763 (1994).
26. Read, R.J. *Acta Crystallogr. A***42**, 140–149 (1986).
27. Brünger, A.T. *XPLOR, V3.1* (Yale University Press, New Haven, Connecticut; 1992).
28. Jones, T.A., Zou, J.Y., Cowan, S.W. & Kjeldgaard, M. *Acta Crystallogr. A***47**, 110–119 (1991).
29. Evans, S.V. *J. Mol. Graphics* **11**, 131–138 (1993).
30. Kraulis, P.J. *J. Appl. Crystallogr.* **24**, 946–950 (1991).
31. Nicholls, A., Sharp, K. and Honig, B. *Proteins* **11**, 281ff (1991).

A gradual disruption of tight side-chain packing: 2D ^{1}H-NMR characterization of acid-induced unfolding of CHABII

Jianxing Song[1,2], Nadège Jamin[1], Bernard Gilquin[1], Claudio Vita[1] and André Ménez[1]

[1]*Département d'Ingénierie et d'Etudes des Protéines, CEA, Saclay, 91191 Gif-sur-Yvette Cedex, France.* [2]*Present address: Biotechnology Research Institute, National Research Council, 6100 Royalmount Avenue, Montreal, Quebec H4P 2R2, Canada.*

Little is known about the mechanism of the transition between native proteins and partially folded intermediates. Complete assignments of 2D ^{1}H-NOESY spectra of CHABII at 5 °C, pH 6.3, 5.5, 4.6 and 4.0, reveal that lowering of pH results in an extensive but gradual disappearance of NOEs, implying a gradual disruption of tight side-chain packing. Moreover, a tertiary packing core is identified at 5 °C and pH 4.0, characterized by persistent long-range NOEs. Thus, we suggest that severe disruption of tight side-chain packing of CHABII can occur at a stage where its secondary structure and tertiary topology remain highly native-like.

Native proteins differ from partially folded ones in tight side-chain packing and extensive tertiary interactions[1–3], which give rise to nuclear Overhauser effects (NOEs) in NMR spectroscopy, thus allowing determination of solution structures[4,5]. By contrast, as a result of their intrinsic flexibility and rapid interconversion between multiple conformations, detection of NOEs in partially folded intermediates using 2D NMR experiments has been largely unsuccessful and still remains a special challenge[6,7]. In particular, the transition between native protein and partially folded intermediates has never been well characterized by NMR, and *de novo*-designed proteins can rarely achieve tight side-chain packings[2,3,6,7]. Detailed NMR characterization of the disruption of tight side-chain packing in native proteins may shed light on this mechanism and provide a rationale for the design of native-like proteins.

Here we report a detailed characterization by 2D ^{1}H NMR of an acid-induced transition of CHABII from the native state to partially folded states. CHABII is a two-disulfide derivative of charybdotoxin (ChTX) in which disulfide 13–33 was deleted by replacing half-cysteine residues 13 and 33 with α-aminobutyric acid residues (Aba)[8,9]. ChTX is a small 37-residue protein containing two canonical secondary structures on opposite faces: a triple-stranded antiparallel β-sheet and a short α-helix[10] (Fig. 1*a*). ChTX represents an α/β motif widely shared by scorpion toxins[10], insect defensins[10], plant γ-thionins[11], a sweet-tasting protein and a family of proteinase inhibitors[12], thus illustrating its high amino acid sequence permissiveness[13]. Furthermore, new functional sites have been engineered into this motif[14,15]. Recently, a high-resolution NMR structure of CHABII has been determined from a large set of distance and dihedral angle constraints at 5 °C and pH 6.3 (ref. 8). CHABII adopts a well-defined structure like a conventional native protein with tight side-chain packing. In particular, medium- and long-range NOEs were observed between the hydroxyl proton of Thr 3 and protons of residues Val 5, Aba 33 and Arg 34, indi-